Journal of Energy Storage 78 (2024) 110166

Contents lists available at ScienceDirect

Journal of Energy Storage

journal homepage: www.elsevier.com/locate/est

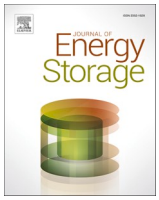

Research papers

Porous carbon materials augmented with heteroatoms derived from hyperbranched biobased benzoxazine resins for enhanced CO_2 adsorption and exceptional supercapacitor performance

Mohsin Ejaz [a], Mohamed Gamal Mohamed [a,b,*], Yu-Ting Chen [a], Kan Zhang [c,**], Shiao-Wei Kuo [a,d,*]

[a] Department of Materials and Optoelectronic Science, Center for Functional Polymers and Supramolecular Materials, National Sun Yat-Sen University, Kaohsiung 804, Taiwan
[b] Department of Chemistry, Faculty of Science, Assiut University, Assiut 71515, Egypt
[c] Research School of Polymeric Materials, School of Materials Science and Engineering, Jiangsu University, Zhenjiang 212013, China
[d] Department of Medicinal and Applied Chemistry, Kaohsiung Medical University, Kaohsiung 807, Taiwan

ARTICLE INFO

Keywords:
Biobenzoxazine
Hyperbranched polymers
Ring-opening polymerization
Porous carbon materials
Supercapacitors

ABSTRACT

Porous carbon materials doped with heteroatoms are an excellent alternative for applications in CO_2 adsorption and supercapacitors. Herein, we present a new approach to obtain heteroatoms (N, O, and S) doped porous carbon materials using bio-based hyperbranched benzoxazine (RES-HP-BZ) as a precursor. Two types of porous carbon materials, poly(RES-HP-BZ)-700 and poly(RES-HP-BZ)-800, were synthesized through a simple calcination method by carbonization and KOH activation of benzoxazine at temperatures of 700 °C and 800 °C, respectively. The chemical structure, texture properties, and surface chemistry characteristics were validated through FTIR, NMR, SEM, XRD, and XPS, respectively. The resulting poly(RES-HP-BZ)-800 exhibited micro and *meso* porous characteristics with a high S_{BET} of 841 $m^2\ g^{-1}$, pore size of 1.14 nm, and pore volume of 0.70 $cm^3\ g^{-1}$. The poly(RES-HP-BZ)-800 also showed a high graphitization degree and electrochemically energetic N-6, N-5, N-Q, O-2, and O-3 heteroatoms, which led to a high capacitance of 523 F g^{-1} (at 0.5 A g^{-1}) as well as CO_2 capture of 4.63 mmol g^{-1} at 298 K. These newly developed bio-based porous carbons derived from hyperbranched bio-benzoxazine with excellent electrochemical performance make them a promising candidate for eco-friendly supercapacitors.

1. Introduction

Recently, the energy crisis has emerged as a foremost global concern due to the significant disparity between escalating energy requirements and the pervasive lack of energy supply [1–5] On the other hand, the recurrent rapid depletion of fossil fuels has given rise to numerous pressing environmental problems that require immediate resolution [6–8]. Consequently, the imperative of creating secure and efficient energy storage methods has become crucial. Various technologies have been devised and put into practice for energy storage, including batteries and supercapacitors [9–12].

Supercapacitors (SCs) are environmentally friendly energy storage solutions that have been steadily increasing in popularity [13–17]. The widespread utilization of SCs can be attributed to their cost-effective maintenance and impressive power density, despite their drawback of limited energy density [18–23]. Enhancing energy density while upholding a high power density holds paramount importance, and the selection of an appropriate electrode material plays a pivotal role in this endeavor [24–28]. Specifically, the heteroatoms doped porous carbons are a favorable choice and showcase remarkable capabilities when they possess abundant porosity, elevated conductivity, and a substantial specific surface area (S_{BET}) [29–33]. As electron contributors within carbon materials, heteroatoms can offer additional redox-active surfaces conducive to energy storage [34,35]. Leveraging these exceptional

* Corresponding authors at: Department of Materials and Optoelectronic Science, Center for Functional Polymers and Supramolecular Materials, National Sun Yat-Sen University, Kaohsiung 804, Taiwan.
** Corresponding author.
E-mail addresses: magamal.eldin12@yahoo.com (M.G. Mohamed), zhangkan@ujs.edu.cn (K. Zhang), kuosw@faculty.nsysu.edu.tw (S.-W. Kuo).

https://doi.org/10.1016/j.est.2023.110166
Received 20 September 2023; Received in revised form 6 December 2023; Accepted 14 December 2023
Available online 22 December 2023

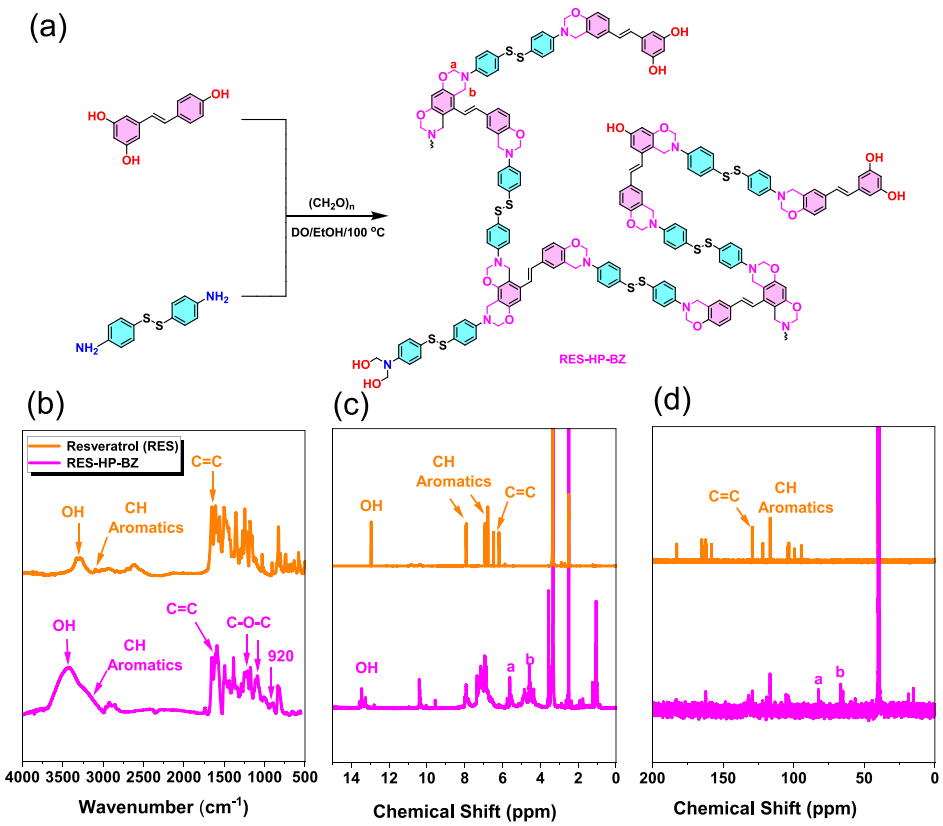

Fig. 1. (a) Synthesis of RES-HP-BZ (b) FTIR (c) ^{1}H NMR (d) ^{13}C NMR of resveratrol and RES-HP-BZ.

attributes, porous carbon materials doped with heteroatoms have the potential to serve as excellent contenders for applications in CO_2 adsorption and supercapacitors.

Benzoxazine (BZ), a thermosetting resin presents a favorable option as a porous carbon precursor due to its substantial nitrogen and oxygen content within the oxazine ring. By utilizing cost-effective raw materials like various phenols, primary amines, and formaldehyde, it becomes straightforward to produce polybenzoxazine (PBZ) thermosetting polymers [36–40]. Consequently, the composition and nature of heteroatoms within polybenzoxazines (PBZs) can be conveniently modified through the substitution of monofunctional amines or phenols with bifunctional compounds. The presence of heteroatoms in the benzoxazine structure can impart carbon materials with a broader range of applications and improved performance [41–43]. Currently, many of the prevalent precursors are employed in the development of N-doped porous carbon materials featuring triazine or amine structures. However, some of these precursors exhibit limited N atom content due to constraints in their structural design and the selectivity of raw materials. Numerous research findings have highlighted the pivotal role played by heteroatoms in supercapacitor electrodes [43,44] [45–48]. These substances are recognized for enhancing the conductivity of carbon-based materials and facilitating the interaction between the electrode material and electrolyte. BZ has emerged as a favorable contender for a precursor of carbon materials due to its oxazine ring configuration, encompassing both N and O atoms. These characteristics contribute to enhancing the variability of heteroatom incorporation [49–53].

Recently, numerous studies have employed benzoxazine for the synthesis of heteroatoms (N and O) porous carbon. For instance, Jiang et al. prepared porous carbons derived from synthesized bio polybenzoxazines having a capacity of 216 F g^{-1} (determined at 0.5 A g^{-1}) [54]. Shi et al. also used bioresources to synthesize material with N, O, and S atoms and this material displayed a capacitance of 310 F g^{-1} at 0.1 A g^{-1} and CO_2 absorbance of 6.78 mmol g^{-1} [55]. The widespread use of fossil fuels today not only harms the environment but also poses a serious risk to human health. Consequently, it holds paramount importance to investigate alternative materials that are both sustainable and eco-friendly, aiming to substitute petroleum-derived products, at least in part [56–58]. The transformation of renewable resources into biofuels, chemicals, and beneficial materials is widely considered a key approach for fostering sustainable progress. Seemingly, employing natural resources directly offers the benefits of simplicity and ease. Nonetheless, this approach encounters a challenge in terms of limited control over structure due to the inherent instability and non-uniformity of these resources. Consequently, predicting or regulating the configurations of resulting porous carbons becomes arduous. In contrast to this, biobased polymers possess distinct molecular structures and exceptional sustainability. This characteristic not only addresses the limitations associated with natural resources but also preserves their advantageous attributes simultaneously.

In this work, we synthesized bio-based hyperbranched benzoxazine using resveratrol (a biobased triphenol), 4,4′-disulfanediyldianiline, and formaldehyde by simple Mannich condensation reaction. Porous carbons doped with heteroatoms such as N, O, and S were synthesized through carbonization, followed by activation using KOH at two distinct temperatures: 700 °C and 800 °C. These materials were denoted as poly (RES-HP-BZ)-700 and poly(RES-HP-BZ)-800, respectively. Notably, the bio-based electrode material poly(RES-HP-BZ)-800 showed a significant S_{BET} of 841 m^2 g^{-1}, the specific capacitance of 523 F $g^{-1,}$ and CO_2 absorbance (4.63 mmol g^{-1}), respectively. This is the first example of the development of N, O, and S heteroatoms doped porous carbon material from hyperbranched benzoxazines as electrode material for supercapacitors. Furthermore, supercapacitors have gained recognition as a power source that aligns with environmental considerations. If it becomes possible to obtain their electrode materials from biobased sources, it will pave the way for realizing a “green + green” strategy. This achievement would mark a significant advancement in the

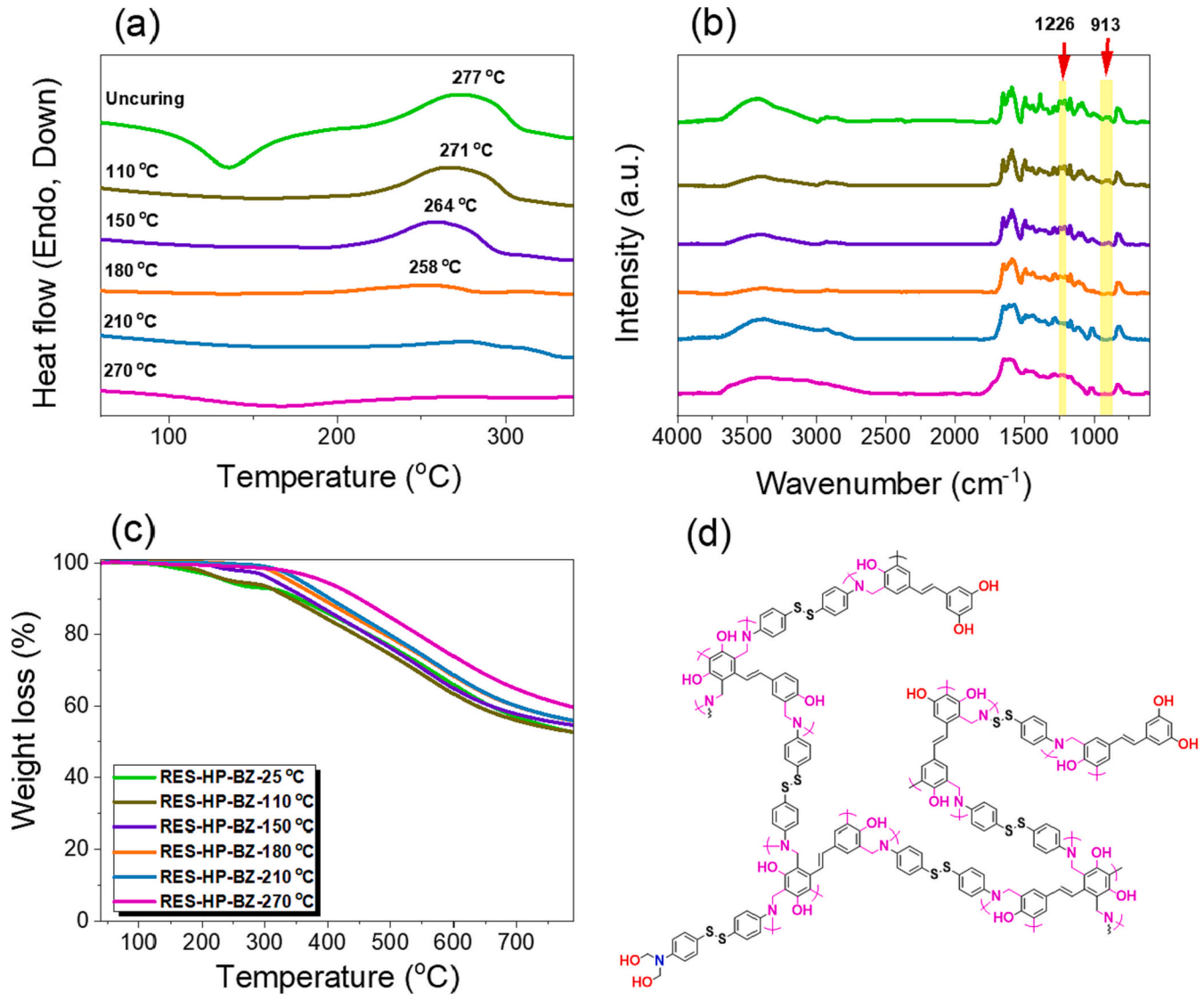

Fig. 2. (a) DSC, (b) FTIR, and (c) TGA analyses of RES-HP-BZ after thermal ROP at different temperatures. (d) Possible thermal ROP of RES-HP-BZ to form poly(RES-HP-BZ).

direction of sustainable development, and it stands as the primary goal of this research.

2. Experimental section

2.1. Materials

Resveratrol (RES), 4,4′-disulfanediyldianiline, and para-formaldehyde $(CH_2O)_n$ were purchased from Alfa Aesar. Absolute Ethanol (EtOH), 1,4-dioxane (DO), and dichloromethane(DCM) were obtained from Sigma-Aldrich.

2.2. Synthesis of bio-hyperbranched benzoxazine (RES-HP-BZ)

Resveratrol (1.00 g, 4.38 mmol), 4,4′-disulfanediyldianiline (1.10 g), and paraformaldehyde (0.53 g) were refluxed in 60 mL of DO and 30 mL of absolute ethanol at 90 °C for 24 h. The unreacted monomers were removed by filtration and performed rotary to solution mixture. Add DCM to get a yellow solid. FTIR (KBr, cm^{-1}): 3421 (hydroxyl group), 3154 (aromatic carbons), 1636 (resveratrol moiety, C═C) 1220 and 1086 (C-O-C), and 920 (benzoxazine ring). ^{1}H NMR: 13.3 (-OH), 7.8–6.9 (aromatic carbons), 84.3–81.2 ppm (OCH_2N) and 67.2–64.1 ppm ($ArCH_2N$).

2.3. Preparation of N, O, and S-doped porous carbon materials from hyperbranched benzoxazines

Firstly, the RES-HP-BZ (3.00 g) was cured at 270 °C for 2 h and then calcinated for 4 h at 600 °C in a furnace. The obtained carbon material was added in KOH/poly(RES-HP-BZ) [1:1] and stirred for 6 h at RT. The liquid solution was removed by rotary and dried the resulting solid in the vacuum oven. Finally, the carbon sample was separately activated in the furnace at 700 °C and 800 °C for 8 h to obtain poly(RES-HP-BZ)-700 and poly(RES-HP-BZ)-800 respectively [Fig. S1].

3. Result and discussion

3.1. Synthesis and characterizations of RES-HP-BZ

We prepared RES-HP-BZ through a simple Mannich condensation of resveratrol, 4,4′-disulfanediyldianiline, and $(CH_2O)_n$ at 100 °C as shown in Fig. 1(a). The chemical structure of RES-HP-BZ was validated from FTIR and NMR spectroscopy. The FTIR spectra of resveratrol showed peaks at 3341, 3092, and 1641 cm^{-1} for OH, CH aromatic, and C═C

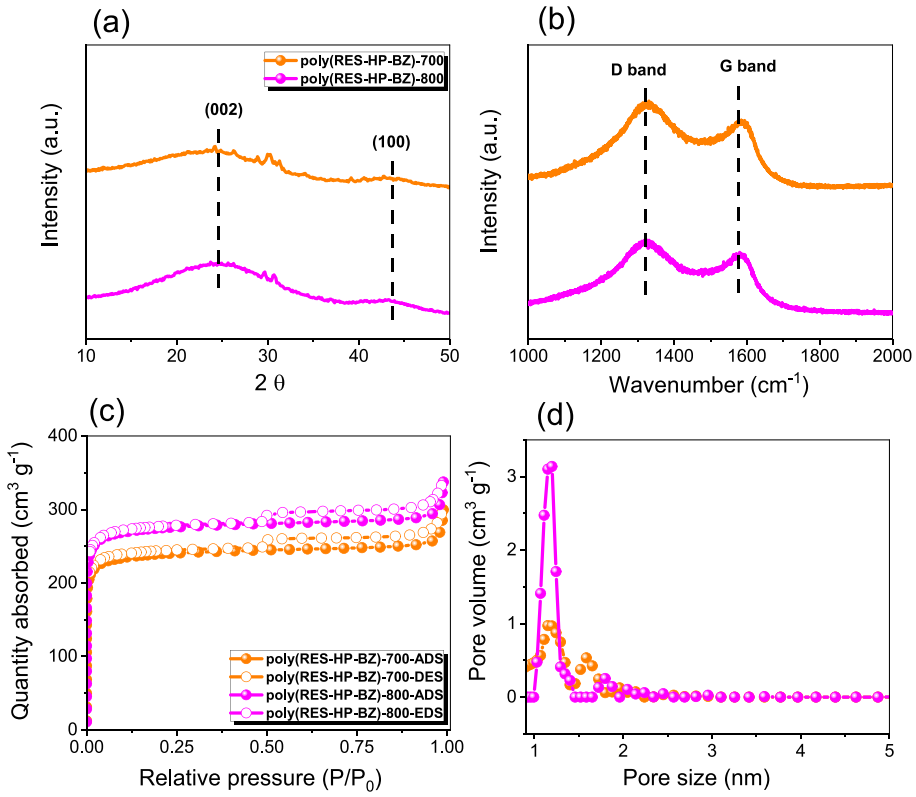

Fig. 3. (a) XRD, (b) Raman, (c) N_2 adsorption/desorption isotherms, and (d) pore size of poly(RES-HP-BZ)-700, of poly(RES-HP-BZ)-800.

Table 1
The XPS fitted data of poly(RES-HB-BZ)-700 and poly(RES-HB-BZ)-800.

Sample	N-6 (375.03 eV)	N-5 (378.01 eV)	N-Q (380.03 eV)	N-X (383.06 eV)	O-1 (531.2 eV)	O-2 (532.12 eV)	O-3 (534.4 eV)
Poly(RES-HP-BZ)-700	26.50	32.95	27.87	12.66	42.78	38.91	18.29
Poly(RES-HP-BZ)-800	26.64	33.29	28.65	11.41	36.23	41.13	22.63

units, respectively [Fig. 1(b)]. The spectrum of RES-HP-BZ featured absorbance bands at 3421 cm^{-1} (residual terminal hydroxyl group), 3154 cm^{-1} (aromatic carbons), 1636 cm^{-1} (resveratrol moiety) 1220 cm^{-1} (symmetric C-O-C), and 920 (benzoxazine ring) [Fig. 1(b)]. We evaluated and compared the NMR analysis [^{1}H and ^{13}C NMR of RES with RES-HP-BZ [Fig. 1(c)]. The ^{1}H NMR of RES-HP-BZ showed chemical shift peaks at 13.3 ppm (residual terminal hydroxyl group), 10.3–6.8 ppm (resveratrol moiety), 5.8–5.4 ppm (OCH_2N), and 4.9–4.3 ppm ($ArCH_2N$), respectively. The signal splitting for both the OCH_2N and $ArCH_2N$ groups was observed, resulting from the asymmetrical chemical environments indicating the branched structure of RES-HP-BZ [59,60]. The ^{13}C NMR spectra of RES-HP-BZ also demonstrated resveratrol moiety and splitting of peaks at 84.3–81.2 ppm (OCH_2N) and 67.2–64.1 ppm ($ArCH_2N$) groups [Fig. 1(d)]. The existence of BZ rings in the RES-HP-BZ is confirmed by NMR spectroscopy.

The thermal ring-opening polymerization (ROP) behavior of RES-HP-BZ was investigated by DSC, IR, and TGA at different curing temperatures [Fig. 2]. The DSC curve of uncured Res-HP-BZ showed two distinct thermal processes, an endothermic melting at 133 °C and an exothermic curing peak at 277 °C [Fig. 2(a)]. After thermal treatment at various temperatures, the endothermic melting peak disappears, and the exothermic curing peak shifts to lower temperatures. After curing of RES-HP-BZ at 110 °C, 150 °C, and 180 °C, the curing peaks were observed as 271 °C, 264 °C, and 258 °C respectively [Fig. 2(a)]. The observed behavior suggests that the thermal treatment caused a partial polymerization of RES-HP-BZ, which consequently affected its subsequent ROP process as well. The ring opening polymerization was observed at 250 °C and 270 °C due to the complete absence of an exothermic curing peak, leading to the formation of poly(RES-HP-BZ). In Fig. 2(a), We measured the thermal polymerization of the Res-HP-BZ using FTIR at various temperatures between 25 and 270 °C [Fig. 2 (b)]. We specifically examined the oxazine ring to assess the ROP behavior of the hyperbranched polymer. As the temperature increased to 180 °C, the intensity at 1226 and 913 cm^{-1} reduced, and with further temperature increments, the oxazine peak vanished entirely, indicating ROP leads to create a poly(RES-HP-BZ) that is more stable under high temperature and has better cross-linking. As a result, the ROP of the BZ ring at 210 °C and 270 °C was verified by DSC and FTIR studies. Furthermore, we investigated the thermal stability of RES-HP-BZ at different curing temperatures using TGA analysis [Fig. 2(c)]. The T_{d10} and char yield for the uncured RES-HP-BZ were 354 °C and 52 wt%, respectively. After undergoing thermal treatment at 270 °C, the RES-HP-BZ monomer's thermal stability and char yield improved to 451 °C and 59 wt%, respectively. The enhanced thermal stability is primarily due to the formation of a high cross-linking poly(RES-HP-BZ) structure with reduced moisture content at high temperatures, resulting from the ROP and the additional polymerization of the C═C groups found in resveratrol [61]. Fig. 2(d) shows the possible ROP of RES-HP-BZ to form poly (RES-HP-BZ). The XRD and Raman spectra are utilized to examine the graphitic characteristics of the carbon samples, poly(RES-HB-BZ)-700 and poly(RES-HB-BZ)-800. The XRD spectra of both carbon materials showed two broad peaks at 25° and 44° corresponding to (002) and

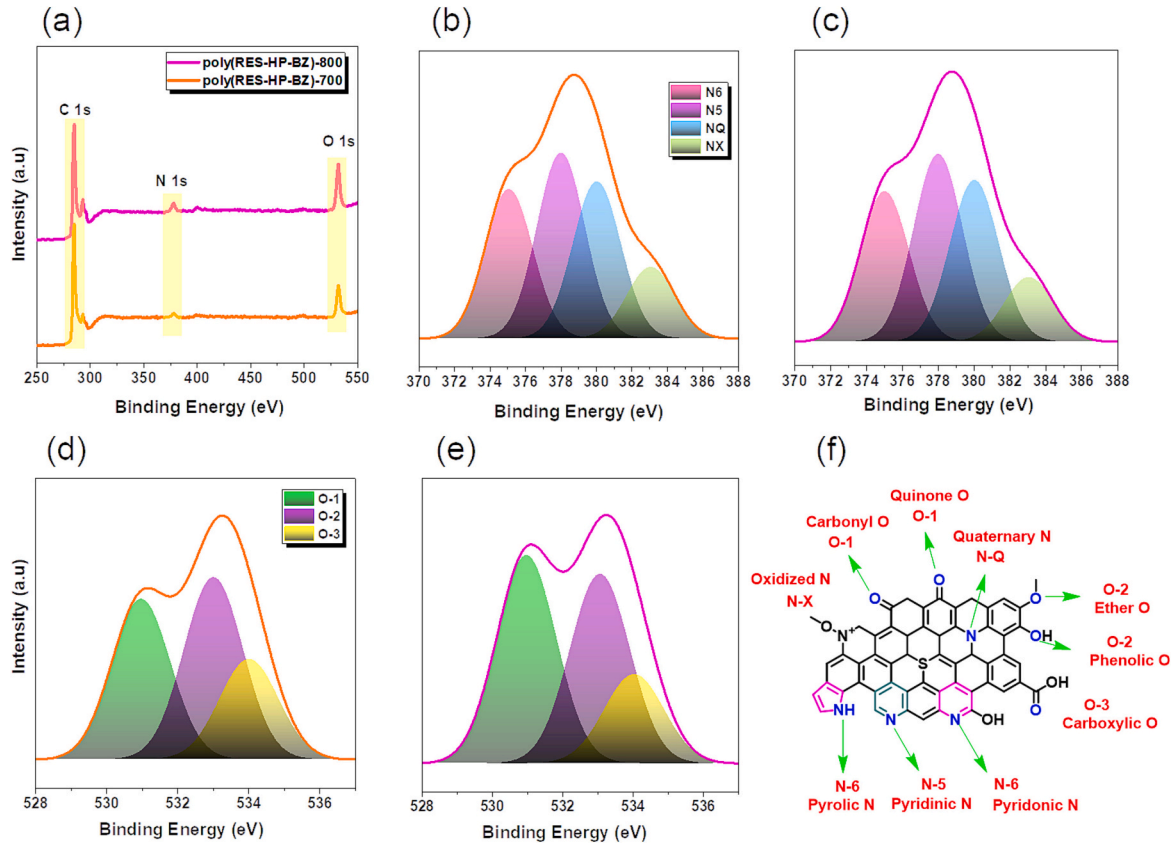

Fig. 4. (a) XPS spectra, (b) N1s spectra of poly(RES-HP-BZ)-700, (c) N1s spectra of poly(RES-HP-BZ)-800, (d) O1s of poly(RES-HP-BZ)-700, (e) N1s spectra of poly (RES-HP-BZ)-800 and (f) possible nitrogen, oxygen and sulfur-doped porous material.

(100) planes representing graphitic carbon respectively, as presented in Fig. 3(a) [62]. The irregular and amorphous carbons are responsible for the peak observed at 25°, whereas the presence of graphitic carbons is indicated by the signal at 44° [63]. The intensity of peak at 44° for poly (RES-HB-BZ)-800 was increased as compared to the poly(RES-HB-BZ)-700 demonstrating strong graphitic characteristics. In the Raman spectra of these two samples, two prominent peaks corresponding to the D and G bands were observed [Fig. 3(b)]. These peaks were positioned at approximately 1332 cm^{-1} and 1588 cm^{-1} for poly(RES-HB-BZ)-700 and 1325 cm^{-1} and 1582 cm^{-1} for poly(RES-HB-BZ)-800 respectively. The G band is associated with the vibration of sp^2-hybridized carbon within the graphite crystallites, while the D band signifies the presence of defects and disorder in carbon layers [64]. The G-band of poly(RES-HB-BZ)-800 exhibited a greater closeness to that of graphene (1581 cm^{-1}), suggesting that poly(RES-HB-BZ)-800 had a more improved graphenoid structure compared to poly(VFBZ-CN)-700. The ratio of the D/G band intensities, abbreviated as I_D/I_G, provides a quantitative measure of the level of graphitization in carbon materials. The I_D/I_G of poly(RES-HB-BZ)-700 and poly(RES-HB-BZ)-800 were 1.36 and 1.09 respectively, indicating the more dominant graphitic, regular, and less disordered structure of poly(RES-HB-BZ)-800 than poly(RES-HB-BZ)-700. The porosities of polybenzoxazines samples after activation at high temperatures were investigated by N_2 adsorption/desorption isotherms as shown in Fig. 3(c). The isothermal profiles of poly(RES-HB-BZ)-700 and poly(RES-HB-BZ)-800 showed type-1isotherms with rapid N_2 uptakes at low pressure which also increase at high pressure suggesting the presence of micropores and mesopores in both samples. Furthermore, the specific surface area of poly(RES-HB-BZ)-800 (841 m^2 g^{-1}) was observed higher than that of poly(RES-HB-BZ)-700 (735 m^2 g^{-1}). According to the pore size distribution curves illustrated in Fig. 3(d), poly (RES-HB-BZ)-700 exhibited a pore size of 1.14 nm and a pore volume of 0.70 cm^{-3} g^{-1}, while poly(RES-HB-BZ)-800 had a pore size of 1.14 nm and a pore volume of 0.74 cm^{-3} g^{-1} (Table S1). In the case of poly(RES-HB-BZ)-800, the elevation in temperature after the KOH activation process resulted in the creation of new micropores and the expansion of pre-existing ultramicropores, thereby augmenting both the surface area and the overall pore volume [63,64]. Through XPS analysis, the chemical composition of the poly(RES-HB-BZ)-800 and poly(RES-HB-BZ)-700 samples after undergoing high-temperature calcination was examined and summarized in Table 1. Additionally, a more in-depth investigation into the chemical states of nitrogen and oxygen molecules present on the surfaces of carbon-based materials was carried out using data analysis fitted with XPS, as depicted in Fig. 4.

The chemical composition of poly(RES-HP-BZ) exhibited a notable abundance of nitrogen (N), oxygen (O), and sulfur (S) atoms within its structure following the (ROP) process, as illustrated in Fig. 2(d). Subsequently, the polymer underwent a 4 h calcination process at 600 °C in a furnace, resulting in the formation of carbon materials characterized by aromatic rings containing N and O atoms. The activation process of carbon precursors using KOH at 800 °C involved several key transformations [3]: (i) KOH effectively reacted with active oxygen-containing species to eliminate O-containing groups. This reaction induced the creation of vacancies, promptly filled by OH- anions from KOH, thereby generating novel oxygen-containing species, including C—O, OH, -O-C-O, and -COOH groups; (ii) Furthermore, KOH could etch carbon fragments, creating specific vacancies that were subsequently occupied by OH–, leading to the formation of new species containing oxygen; (iii) The interaction of KOH with nitrogen atoms in the activated carbon materials resulted in the formation of diverse nitrogen groups, including pyridinic, pyrrolic, quaternary, and oxidized nitrogen species, as depicted in Fig. 4(f). On all sample surfaces, four distinct nitrogen species were identified, including pyridinic nitrogen (N-5 at 375.03 eV), pyrrolic or pyridonic nitrogen (N-6 at 378.01 eV), quaternary nitrogen (N-Q at 380.03 eV), and oxidized nitrogen (N-X at 383.06 eV), as

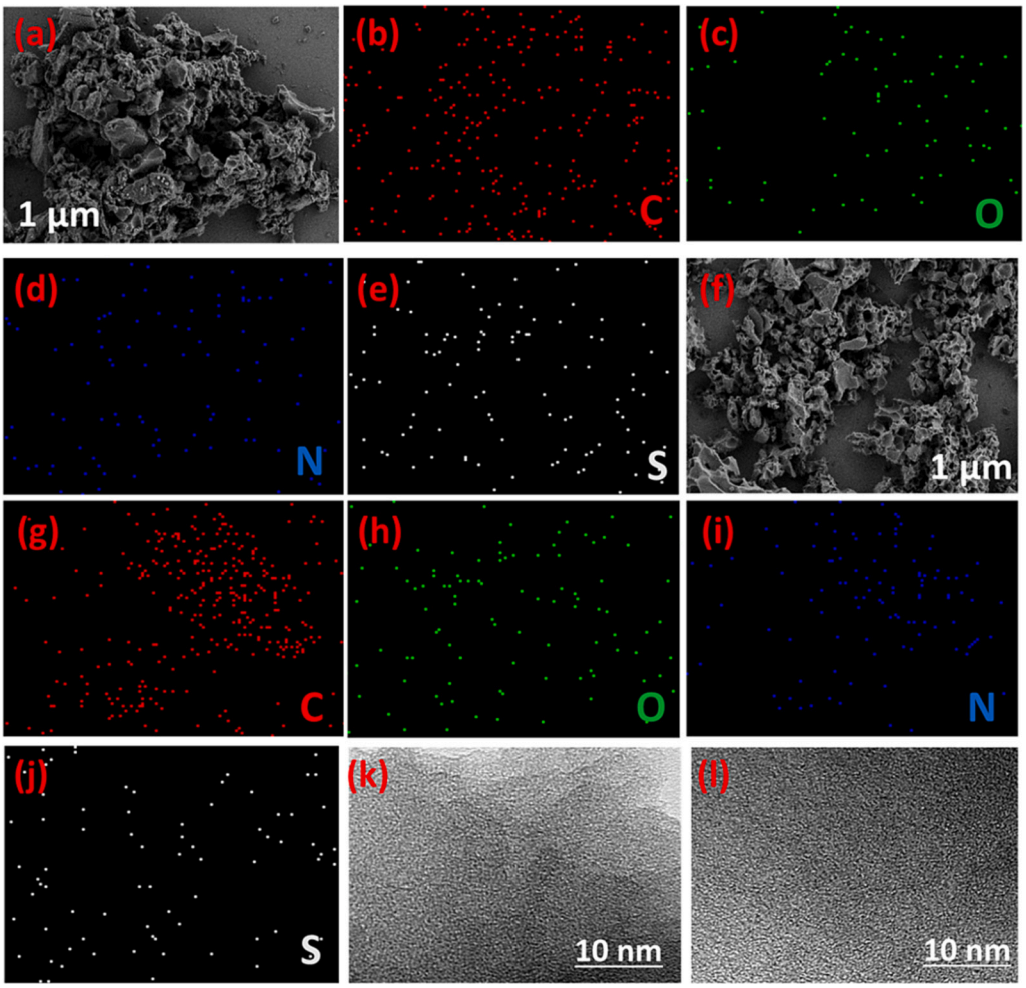

Fig. 5. (a-j) SEM and SEM-EDS images with their corresponding element mapping (C, O, N and S) of poly(RES-HP-BZ)-700 and poly(RES-HP-BZ)-800. (k,l) TEM images of poly(RES-HP-BZ)-700 and poly(RES-HP-BZ)-800.

detailed in Table 1 and illustrated in Fig. 4(a) and (b). It is worth noting that N-6 and N-5 species were predominant across all carbon samples, a phenomenon that can be attributed to the transition between amide units and triazine groups in polybenzoxazines following the calcination process [64]. Furthermore, there is an expectation that N-6 and N-5 will demonstrate high electrochemical efficiency when immersed in an electrolyte solution, resulting in substantial pseudocapacitance that enhances overall capacitance [65]. Additionally, the presence of N-Q, which is bonded to three carbon atoms and integrated into the carbon framework, is anticipated to facilitate electron mobility and enhance the conductivity of carbon-based materials [66]. So, poly(RES-HB-BZ)-800 with a higher concentration of N-Q is expected to have better electrochemical performance than poly(RES-HB-BZ)-700. The three kinds of oxygen species can be observed in both sample surfaces: quinone (O-1 at 531.2 eV), phenolic hydroxyl or ether (O-2 at 532.12 eV), carboxyl (O-3 at 534.4 eV) as shown in Table 1 and Fig. 4(d) and (e). It has been found that although O-2 and O-3 may exhibit pseudocapacitance through reversible redox processes, while O-1 is electrochemically inert [64]. It can be seen that both poly(RES-HB-BZ)-700 and poly(RES-HB-BZ)-800 have dominant O-2 and O-3 species that may generate pseudocapacitance. The XPS analysis suggests our new RES-HP-BZ carbon samples may have good CO_2 capture and electrochemical performances.

3.2. The morphologies of poly(RES-HB-BZ)-700 and poly(RES-HB-BZ)-700

The surface morphology after calcination and KOH activation were analyzed by SEM and TEM [Fig. 5(a-l)]. The SEM images of poly(RES-HB-BZ)-700 and poly(RES-HB-BZ)-800 demonstrated pores on their surfaces due to calcination and KOH activation [Fig. 5(a) and (f)]. The presence of heteroatoms (C, N, O, and S) in poly(RES-HB-BZ)-700 [Fig. 5 (b-e)] and poly(RES-HB-BZ)-800 [Fig. 5(g-j)] were also observed by SEM element mapping. The TEM analysis also showed the existence of porous characteristics in both carbon materials [Fig. 5(k) and 5(l)]. Both SEM and TEM characterizations confirmed the porous structure of poly(RES-HB-BZ)-700 and poly(RES-HB-BZ)-800.

The CO_2 capture performance of poly(RES-HB-BZ)-700 and poly (RES-HB-BZ)-800 are shown in Fig. 6(a). The poly(RES-HB-BZ)-800 experienced higher CO_2 capture at 25 °C (4.63 mmol g^{-1}) than poly (RES-HB-BZ)-700 (4.41 mmol g^{-1}) attributed to its higher nitrogen content, surface area, pore volume, and average pore size. The CO_2 capture of any material depends upon the physical and chemical adsorption Fig. 6(b) [67]. In physical adsorption, the CO_2 molecules adsorbed on the carbon through van der Wall forces and promote CO_2 capture performance by pore-filling mechanism. The surface area and pore volume of poly(RES-HB-BZ)-800 was high promoting more pore-filling mechanism than poly(RES-HB-BZ)-700. Furthermore, in terms of chemical adsorption, the poly(RES-HB-BZ)-800 has a higher N content in its structure leading to superior hydrogen bonding interaction

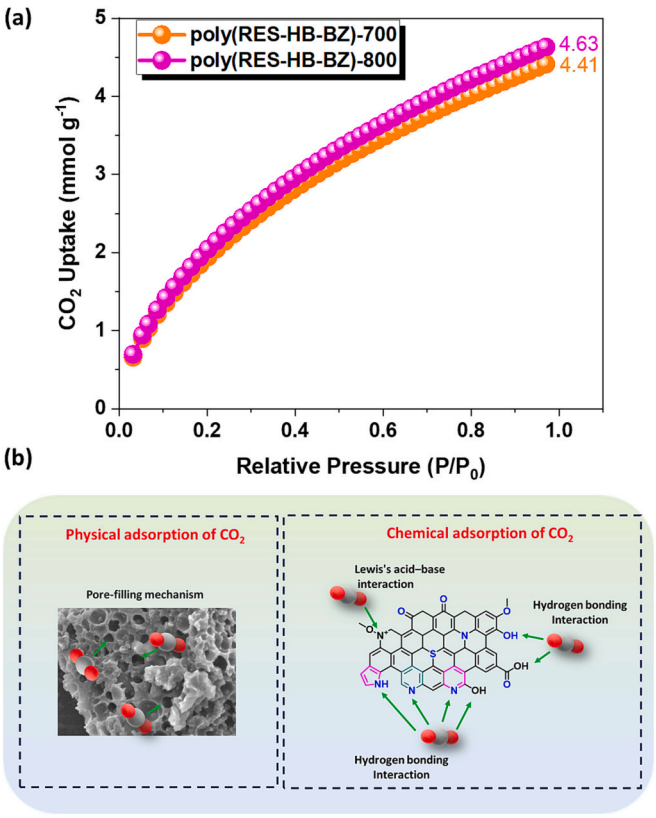

Fig. 6. (a) CO_2 capture of poly(RES-HP-BZ)-700 and poly(RES-HP-BZ)-800 at 25 °C and (b) possible CO_2 capture mechanisms of porous carbons.

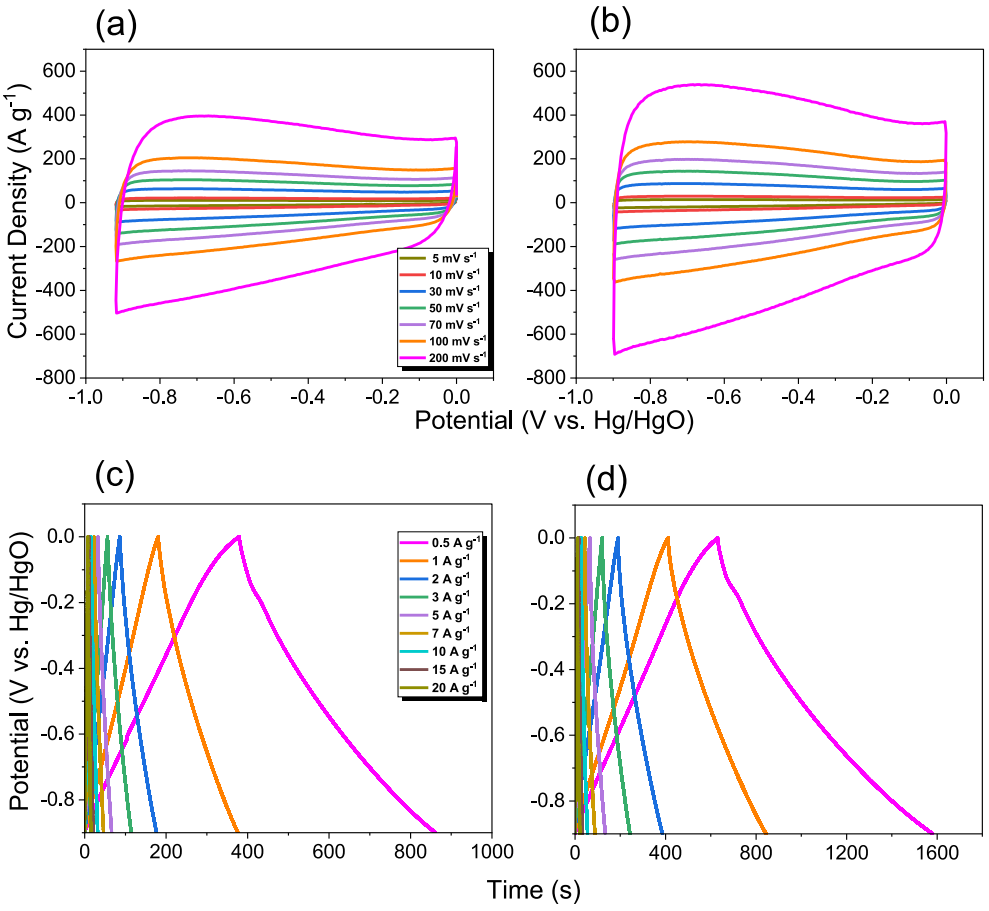

Fig. 7. (a, b) CV curves and (c, d) GCD curves of poly(RES-HP-BZ)-700 and poly(RES-HP-BZ)-800.

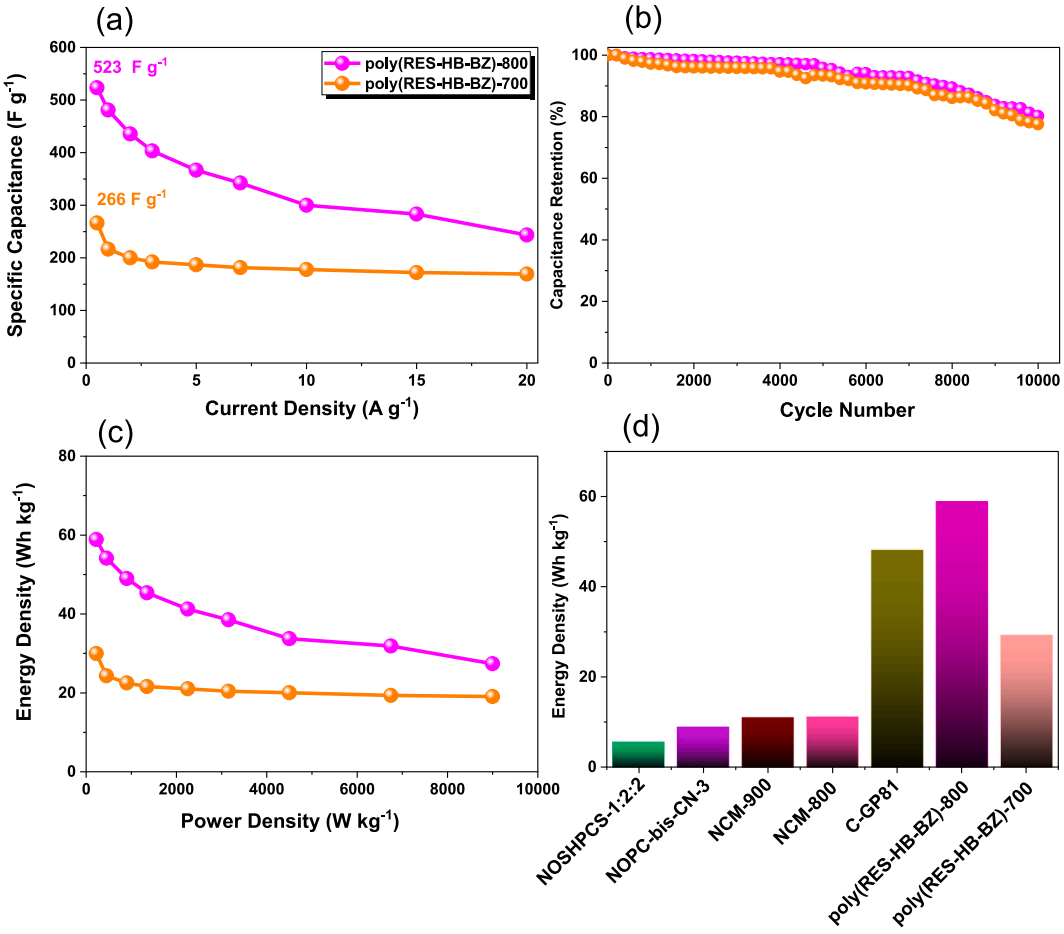

Fig. 8. (a) Specific Capacitance (b) Cyclic stability (c) Ragone plot of poly(RES-HP-BZ)-700 and poly(RES-HP-BZ)-800 (d) Comparison of energy density with other porous materials.

(OH$^{\cdots}$ = O-C=O) and Lewis acid-base interaction (N$^{+\cdots}$ =O-C=O) with CO_2 molecules [67]. These chemical interactions also account for promoting the superior CO_2 adsorption capacity of poly(RES-HB-BZ)-800 than that of poly(RES-HB-BZ)-700. Table S2 shows the comparison of CO_2 capture performance of poly(RES-HB-BZ)-700 and poly(RES-HB-BZ)-800 and other N-doped carbon materials.

3.3. Electrochemical performances of poly(RES-HB-BZ)-700 and poly (RES-HB-BZ)-800

The electrochemical performances of both poly(RES-HB-BZ)-700 and poly(RES-HB-BZ)-800 microporous carbon materials were evaluated in 6 M KOH aqueous electrolyte using three-electrode configurations. The CV profiles of both samples showed quasitriangular shapes with humps suggesting EDLC and pseudocapacitance [Fig. 7(a) and (b)] [68]. The CV loops of poly(RES-HB-BZ)-800 have a higher area than that of poly(RES-HB-BZ)-700 due to its higher surface area and pore volume, suggesting higher specific capacitance performance. The CV profile curves remain the same at lower scan rates, demonstrating their high stability and capacitance performance [69]. The galvanostatic charge-discharge (GCD) profiles of both samples were investigated, as shown in Fig. 7 (c) and (d). The GCD curves of both electrode materials are almost triangular with a minor curvature, which is indicative of high capacitance and strong electrochemical reversibility. The triangular curves with minor curvatures suggest the presence of both EDLC and pseudocapacitance [70–74]. The presence of pseudocapacitive behavior is caused by Faradaic interactions between the heteroatoms that exist on microporous carbon materials and the electrolyte. The discharge curves of poly(RES-HB-BZ)-800 electrode materials exhibited longer discharge time than poly(RES-HB-BZ)-700 electrode materials which accords with the CV analysis.

The specific capacitance of poly(RES-HB-BZ)-800 and poly(RES-HB-BZ)-700 electrode materials at 0.5 A g^{-1} were observed as 523 F g^{-1} and 266 F g^{-1}; at 20 A g^{-1}, it was 243.2 F g^{-1} and 169.33 F g^{-1}, respectively [Fig. 8(a)]. The high surface area with micro/macropores in poly(RES-HB-BZ)-800 increases the number of charges that can be accumulated in the micropores, their electrochemical accessibility to electrolyte ions, and makes it feasible for electrolyte ions to diffuse quickly at high current densities [63,64]. Additionally, the larger concentrations of electrochemically energetic N-6, N-5, N-Q, O-2, and O-3 heteroatoms in the poly(RES-HB-BZ)-800 electrode result in higher performance. Therefore, the specific capacitance of poly(RES-HB-BZ)-800 electrode in all current densities is higher than that of poly(RES-HB-BZ)-700 electrode [Fig. 8(a)]. Interestingly, the exceptional specific capacitances of poly (RES-HB-BZ)-700 and poly(RES-HB-BZ)-800 outperform those of previously described N-doped carbon materials such as VCF5g (310 F g^{-1} at 0.1 A g^{-1}) [55], poly(VFBZ-CN)-700 (408 F g^{-1} at 0.5 A g^{-1}) [75], NOSHPCs-1:2:2 (216.5 F g^{-1} at 0.5 A g^{-1}) [54], NOPC-bis-CN-3 (167.3 F g^{-1} at 1 A g^{-1}) [63], NPC-600 (254.4 F g^{-1} at 1 A g^{-1}) [64] and NCM-900 (460 F g^{-1} at 0.25 A g^{-1}) [53] (Table S3). The cyclic stabilities of poly(RES-HB-BZ)-700 and poly(RES-HB-BZ)-800 were evaluated at 20 A g^{-1} over 10,000 cycles [Fig. 8(b)]. Both electrode materials showed excellent stability of 77.56 % and 80.23 % to their initial capacitance respectively. The Ragone plot of poly(RES-HB-BZ)-700 and poly(RES-HB-BZ)-800 is displayed in Fig. 8(c). The poly(RES-HB-BZ)-800 material exhibited an impressive energy density of 58.8 Wh kg^{-1}, which

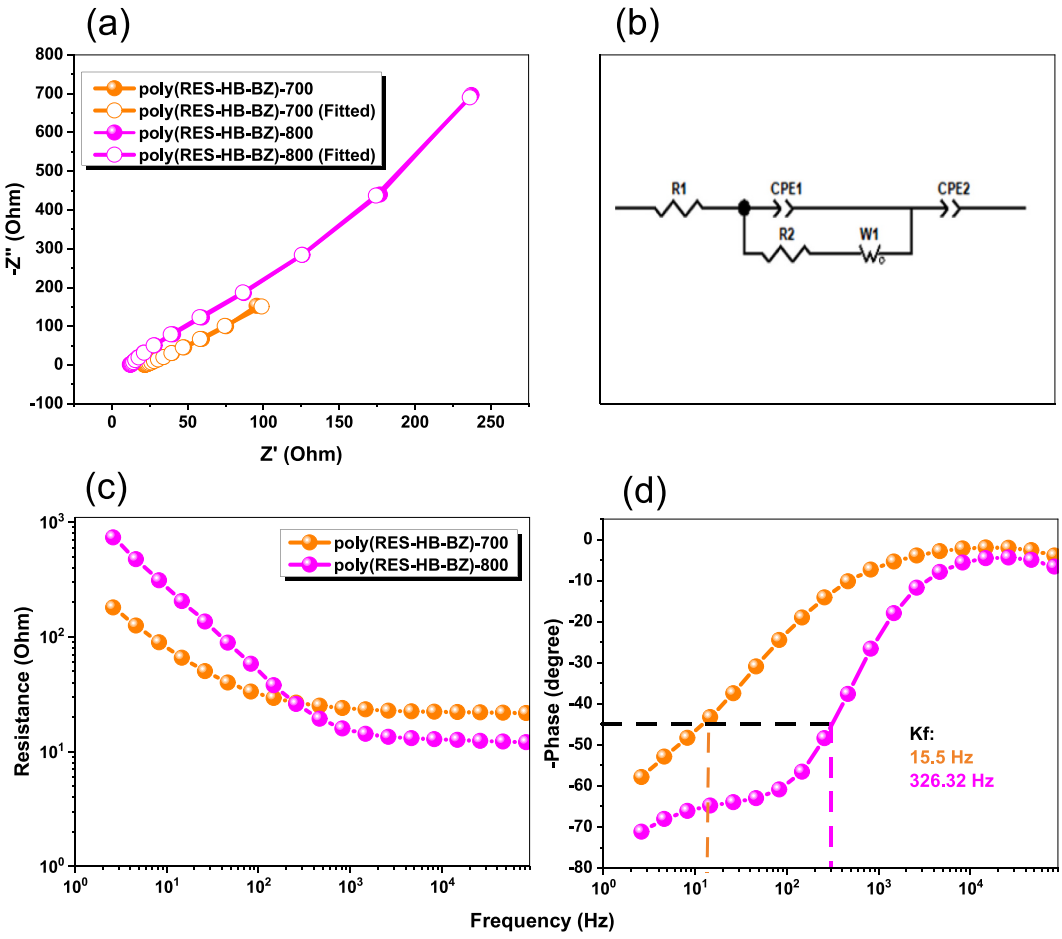

Fig. 9. Electrochemical impedance spectrometry curves: (a) Nyquist plots and (b) equivalent fitted circuit, (c) Bode plot of frequency-dependent resistance (magnitude), and (d) Bode plot of frequency-dependent phase angles of poly(RES-HP-BZ)-700, and poly(RES-HP-BZ)-800.

corresponds to a power density of 225 W kg^{-1}. Notably, even at a high-power density of 9000 W kg^{-1}, it maintained a substantial energy density of 27.36 Wh kg^{-1}. This sample stands out as having the highest energy density among all the porous materials tested, as illustrated in Fig. 8(d). This outstanding energy density and power density of poly (RES-HB-BZ)-800 is due to its high surface area, porosity, and hetero-atoms. Particularly, the porous structures can help ions move around, and the heteroatoms can improve both the capacitance and the electrical transmission providing poly(RES-HB-BZ)-800 great electrochemical performance. Further investigation into the electrochemical properties of poly(RES-HB-BZ)-700 and poly(RES-HB-BZ)-800 porous materials was conducted using electrochemical impedance spectroscopy (EIS) [Fig. 9]. Along with other electrochemical properties like capacitance and resistance, EIS is also helpful in understanding its impedance as a function of frequency. The series resistance of poly(RES-HB-BZ)-700 and poly(RES-HB-BZ)-800 were calculated after fitting data of EIS as 21.15 Ω and 12.17 Ω, respectively [Fig. 9(a) and (b)]. The poly(RES-HB-BZ)-800 had minimum resistance, demonstrating its advantageous qualities for effective electrode material. These two porous materials also have exceptional capacitive capabilities in energy storage devices, as shown by the frequency-dependent magnitude Bode plot (Fig. 9(c)). The frequency-dependent phase-angle Bode graphs for both porous materials are shown in Fig. 9(d), demonstrating the knee frequencies that measure the performance of the porous materials. The knee frequency occurs as the phase angle hits 45°, indicating an equal amount of capacitive and resistive responses. The knee frequencies of poly(RES-HB-BZ)-700 and poly(RES-HB-BZ)-800 were observed as 15.5 Hz and 326.32 Hz respectively. These electrodes exhibited noteworthy knee frequencies, indicating their potential use as energy storage electrode materials. In summary, EIS revealed that both materials have the potential to be used as effective electrode materials in energy storage applications, especially poly(RES-HB-BZ)-800 which has low series resistance.

3.4. Electrochemical performance of poly(RES-HP-BZ)-700, and poly (RES-HP-BZ)-800 based on symmetric coin cell

The three-electrode electrochemical performances of poly(RES-HB-BZ)-700 and poly(RES-HB-BZ)-800 were excellent and can be used as real-life supercapacitors. So, we assembled two electrode symmetric coin cell devices to investigate their practical applications [Fig. 10]. The 6 M KOH electrolyte was used alongside porous carbon [poly(RES-HB-BZ)-700 or poly(RES-HB-BZ)-800] to act as positive and negative electrodes. The CV curves were analyzed at the potential window of (0 to +0.7 V) with various scan rates (5 mV s^{-1} to 200 mV s^{-1}) [Fig. 10(a) and (b)]. The quasitriangular shapes with humps were observed suggesting EDLC and pseudocapacitance behavior without affecting the shape at lower scan rates assisting high-rate capacity [68,69]. The GCD curves at different current densities experienced almost triangular curves indicating EDLC and some pseudocapacitance response [Fig. 10(c) and (d)]. The specific capacitance of poly(RES-HB-BZ)-800 and poly(RES-HB-BZ)-700 at 0.5 A g^{-1} were observed as 244.4 F g^{-1} and 147.3 F g^{-1}; and at 20 A g^{-1} it was 121.1 F g^{-1} and 71.42 F g^{-1}, respectively [Fig. 11(a)]. The Ragone plot of poly(RES-HB-BZ)-800 demonstrated a maximum energy density of 16.63 Wh kg^{-1} at a power density of 346 W kg^{-1} and maintained an energy density of 8.24 Wh kg^{-1} by increasing power density to 13,990 W kg^{-1} [Fig. 11(b)]. The cyclic stabilities of poly(RES-HB-BZ)-

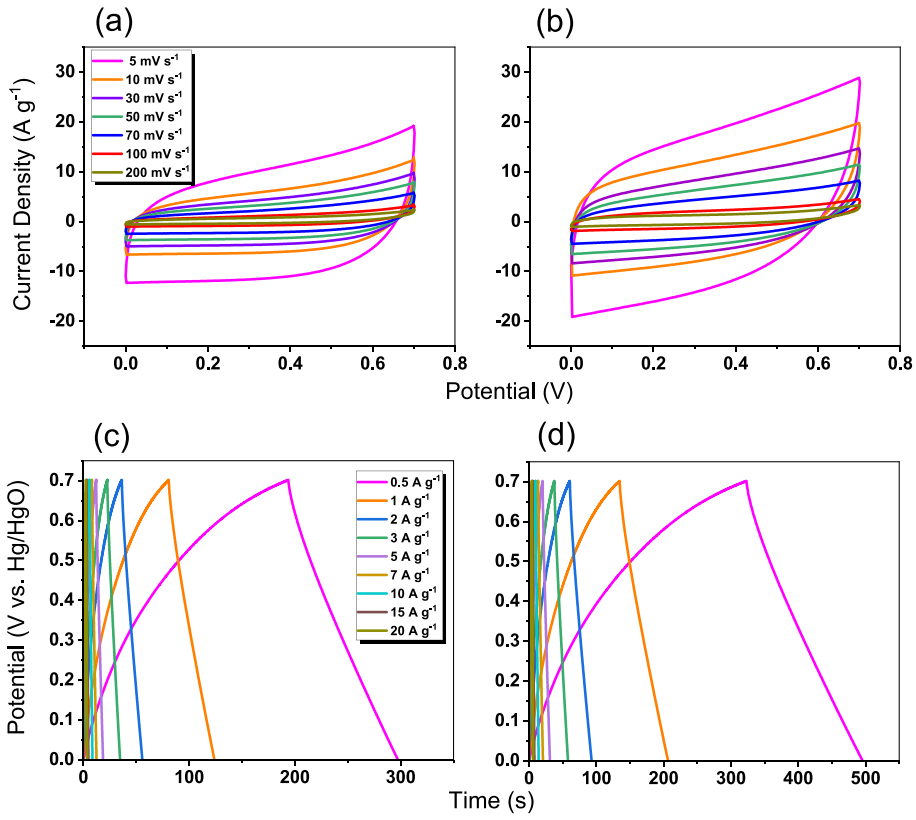

Fig. 10. (a, b) CV curves and (c, d) GCD curves of poly(RES-HP-BZ)-700 and poly(RES-HP-BZ)-800 based on a symmetric coin cell.

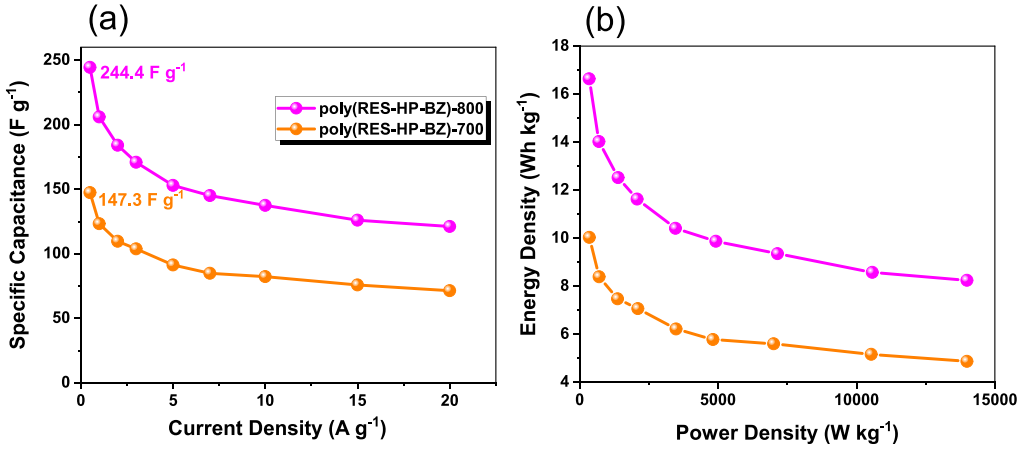

Fig. 11. (a) Specific capacitance and (b) Ragone plot of poly(RES-HP-BZ)-800 and poly(RES-HP-BZ)-700 based on a symmetric coin cell.

700 and poly(RES-HB-BZ)-800 were evaluated at 20 A g^{-1} over 10,000 cycles [Fig. S2]. Both electrode materials showed excellent stability of 75.56 % and 77.47 % to their initial capacitance respectively.

4. Conclusion

We synthesized N, O, and S-doped porous carbon materials through the carbonization of poly(RES-HP-BZ), which is a newly prepared polybenzoxazine based on the bio-based hyperbranched benzoxazine from resveratrol, 4,4′-disulfanediyldianiline, and paraformaldehyde. The excellent thermal stabilities of poly(RES-HP-BZ) were observed which surpassed conventional polybenzoxazine thermosets derived from petroleum resources. The development of N, O, and S heteroatoms doped porous carbon material from hyperbranched benzoxazines demonstrated excellent electrochemical performance and CO_2 absorbance capacity. The poly(RES-HP-BZ)-800 demonstrated a high specific capacitance of 523 F g^{-1}, high energy density of 58 Wh Kg^{-1}, and outstanding capacitance retention of 93 %. This outstanding capacitance is due to the presence of electrochemically energetic heteroatoms after calcination. The CO_2 capture of poly(RES-HP-BZ)-800 was observed as 4.63 mmol g^{-1} at 298 K attributed to its high nitrogen content, and high S_{BET}. In conclusion, porous carbons with outstanding electrochemical and CO_2 absorbance properties have been successfully achieved from biobased resources. The current study exhibits the foundation for the "green materials + green device" concept, which is a significant step towards sustainable development.

CRediT authorship contribution statement

Mohsin Ejaz: Conceptualization, Data curation, Formal analysis, Writing – original draft, Writing – review & editing. **Mohamed Gamal Mohamed:** Conceptualization, Data curation, Formal analysis, Investigation, Methodology, Supervision, Writing – original draft, Writing – review & editing. **Yu-Ting Chen:** Data curation. **Kan Zhang:** Supervision. **Shiao-Wei Kuo:** Supervision.

Declaration of competing interest

The authors declare that they have no known competing financial interests or personal relationships that could have appeared to influence the work reported in this paper.

Data availability

The data that has been used is confidential.

Acknowledgments

This study was supported financially by the Ministry of Science and Technology, Taiwan, under contracts NSTC 110-2124-M-002-013 and 111-2223-E-110-004. The authors thank the staff at National Sun Yat-sen University for their assistance with the TEM (ID: EM022600) experiments.

Appendix A. Supplementary data

Supplementary data to this article can be found online at https://doi.org/10.1016/j.est.2023.110166.

References

[1] Q. Luo, H. Ma, Q. Hou, Y. Li, J. Ren, X. Dai, Z. Yao, Y. Zhou, L. Xiang, H. Du, H. He, N. Wang, K. Jiang, H. Lin, H. Zhang, Z. Guo, All-carbon-electrode-based endurable flexible perovskite solar cells, Adv. Funct. Mater. 28 (2018) 1706777, https://doi.org/10.1002/adfm.201706777.

[2] Q. Wei, F. Xiong, S. Tan, L. Huang, E.H. Lan, B. Dunn, L. Mai, Porous one-dimensional nanomaterials: design, fabrication and applications in electrochemical energy storage, Adv. Mater. 29 (2017) 1602300, https://doi.org/10.1002/adma.201602300.

[3] W. Chen, M. Gong, K. Li, M. Xia, Z. Chen, H. Xiao, Y. Fang, Y. Chen, H. Yang, H. Chen, Insight into KOH activation mechanism during biomass pyrolysis: chemical reactions between O-containing groups and KOH, Appl. Energy 278 (2020), 115730, https://doi.org/10.1016/j.apenergy.2020.115730.

[4] M. Ejaz, M.G. Mohamed, S.W. Kuo, Solid state chemical transformation provides a fully benzoxazine-linked porous organic polymer displaying enhanced CO_2 capture and supercapacitor performance, Polym. Chem. 14 (2023) 2494–2509, https://doi.org/10.1039/d3py00158j.

[5] S. Xiong, J. Liu, Y. Wang, X. Wang, J. Chu, R. Zhang, M. Gong, B. Wu, Solvothermal synthesis of triphenylamine-based covalent organic framework nanofibers with excellent cycle stability for supercapacitor electrodes, J. Appl. Polym. Sci. 139 (2021) 51510, https://doi.org/10.1002/app.51510.

[6] S.Y. Chang, A.M. Elewa, M.G. Mohamed, I.M.A. Mekhemer, M.M. Samy, K. Zhang, H.H. Chou, S.W. Kuo, Rational design and synthesis of bifunctional Dibenzo[g,p]chrysene-based conjugated microporous polymers for energy storage and visible light-driven photocatalytic hydrogen evolution, Mater. Today Chem. 33 (2023), 101680, https://doi.org/10.1016/j.mtchem.2023.101680.

[7] M.G. Mohamed, S.Y. Chang, M. Ejaz, M.M. Samy, A.O. Mousa, S.W. Kuo, Design and synthesis of bisulfone-linked two-dimensional conjugated microporous polymers for CO_2 adsorption and energy storage, Molecules 28 (2023) 3234, https://doi.org/10.3390/molecules28073234.

[8] M.M. Samy, M.G. Mohamed, S.W. Kuo, Conjugated microporous polymers based on ferrocene units as highly efficient electrodes for energy storage, Polymer 15 (2023) 1095, https://doi.org/10.3390/polym15051095.

[9] L.L. Zhang, X.S. Zhao, Carbon-based materials as supercapacitor electrodes, Chem. Soc. Rev. 38 (2009) 2520–2531, https://doi.org/10.1039/B813846J.

[10] C. Liu, Z. Yu, D. Neff, A. Zhamu, B.Z. Jang, Graphene-based supercapacitor with an ultrahigh energy density, Nano Lett. 10 (2010) 4863–4868, https://doi.org/10.1021/nl102661q.

[11] M.G. Mohamed, A.M. Elewa, M.S. Li, S.W. Kuo, Construction and multifunctional of hypercrosslinked porous organic polymers containing ferrocene unit for high-performance iodine adsorption and supercapacitor, J. Taiwan Inst. Chem. Eng. 150 (2023), 105045, https://doi.org/10.1016/j.jtice.2023.105045.

[12] X. Guan, Y. Zhao, H. Pei, M. Zhao, Y. Wang, X. Zhou, M.G. Mohamed, S.W. Kuo, Y. Ye, Metalloporphyrin conjugated porous polymer in-situ grown on a Celgard separator as multifunctional polysulfide barrier and catalyst for high-performance Li-S batteries, Chem. Eng. J. 473 (2023), 144733, https://doi.org/10.1016/j.cej.2023.144733.

[13] X. Chang, C.W. Lin, A. Huang, M.F. El-Kady, R.B. Kaner, Molecular engineering of hierarchical conducting polymer composites for highly stable supercapacitors, Nano Lett. 23 (2023) 3317–3325, https://doi.org/10.1021/acs.nanolett.3c00284.

[14] S.U. Sharma, M.H. Elsayed, I.M.A. Mekhemer, T.S. Meng, H.H. Cho, S.W. Kuo, M. G. Mohamed, Rational design of pyrene and thienyltriazine-based conjugated microporous polymers for high-performance energy storage and visible-light photocatalytic hydrogen evolution from water, Giant 17 (2024) 100217, https://doi.org/10.1016/j.giant.2023.100217.

[15] X. Jiang, X. Wu, Y. Xie, Z. Wang, J. Huang, Y. Qu, D. Mu, X. Zhang, W. Yang, H. Zhang, Additive engineering enables ionic-liquid electrolyte-based supercapacitors to deliver simultaneously high energy and power density, ACS Sustain. Chem. Eng. 11 (2023) 5685–5695, https://doi.org/10.1021/acssuschemeng.3c00213.

[16] X. Han, J. Sun, Q. Li, X. He, L. Dang, Z. Liu, Z. Lei, Highly flexible PEDOT film assembled with solution-processed nanowires for high-rate and long-life solid-state supercapacitors, ACS Sustain. Chem. Eng. 11 (2023) 2938–2948, https://doi.org/10.1021/acssuschemeng.2c06423.

[17] A. Narayanan, A. Siddiqa, N.K. Kodihalli, G. Hegde, D.H. Nagaraju, M. Padaki, Designing of a free-standing flexible symmetric electrode material for capacitive deionization and solid-state supercapacitors, ACS Sustain. Chem. Eng. 11 (2023) 3750–3759, https://doi.org/10.1021/acssuschemeng.2c06817.

[18] M.G. Mohamed, H.Y. Hu, S. Santhoshkumar, M. Madhu, T.H. Mansoure, C. W. Hsiao, Y. Ye, C.W. Huang, W.L. Tseng, S.W. Kuo, Design and synthesis of bifunctional conjugated microporous polymers containing tetraphenylethene and bisulfone units for energy storage and fluorescent sensing of p-nitrophenol, Colloids Surf. A Physicochem. Eng. Asp. 600 (2024), 132675, https://doi.org/10.1016/j.colsurfa.2023.132675.

[19] X. Yan, Y. He, X. Liu, S. Jing, J. Guan, W. Gao, S. Ray, Y. Xiong, T. Li, X. Ge, Deterministic effect of the solid-state diffusion energy barrier for a charge carrier on the self-discharge of supercapacitors, ACS Sustain. Chem. Eng. 8 (2023) 2376–2384, https://doi.org/10.1021/acsenergylett.3c00453.

[20] H. Aydın, U. Kurtan, B. Üstün, S.N. Koç, E. Akgül, M. Demir, A review on the recent advancement of metal-boride derived nanostructures for supercapacitors, J. Energy Storage 72 (2023), 108306, https://doi.org/10.1016/j.est.2023.108306.

[21] S. Satpathy, N.K. Misra, D.K. Shukla, V. Goyal, B.K. Bhttacharyya, C.S. Yadav, An in-depth study of the electrical characterization of supercapacitors for recent trends in energy storage system, J. Energy Storage. 57 (2023), 106198, https://doi.org/10.1016/j.est.2022.106198.

[22] T. Kavinkumar, G. Jang, A.T. Sivagurunathan, D.H. Kim, Reconfiguration of the electronic structure of metal phosphide for ultrahigh energy density hybrid supercapacitors, Chem. Eng. J. 470 (2023), 144214, https://doi.org/10.1016/j.cej.2023.144214.

[23] P.N. Singh, M.G. Mohamed, S.V. Chaganti, S.U. Sharma, M. Ejaz, J.T. Lee, S. W. Kuo, Rational design of ultrastable conjugated microporous polymers based on pyrene and perylene units as high-performance organic electrode materials for supercapacitor applications, ACS Appl. Energy Mater. 6 (2023) 8277–8287, https://doi.org/10.1021/acsaem.3c01391.

[24] L. Li, J. Meng, M. Zhang, T. Liu, C. Zhang, Recent advances in conductive polymer hydrogel composites and nanocomposites for flexible electrochemical supercapacitors, Chem. Commun. 58 (2021) 185–207, https://doi.org/10.1039/d1cc05526g.

[25] B. Zhang, C. Zhang, W. Yuan, O. Yang, Y. Liu, L. He, Y. Hu, L. Zhou, J. Wang, Z. L. Wang, Highly stable and eco-friendly marine self-charging power systems composed of conductive polymer supercapacitors with seawater as an electrolyte, ACS Appl. Mater. Interfaces 14 (2022) 9046–9056, https://doi.org/10.1021/acsami.1c22129.

[26] M.M. Samy, M.G. Mohamed, S.U. Sharma, S.V. Chaganti, J.T. Lee, S.W. Kuo, An Ultrastable Tetrabenzonaphthalene-linked conjugated microporous polymer functioning as a high-performance electrode for supercapacitors, J. Taiwan Inst. Chem. Eng. (2023), 104750, https://doi.org/10.1016/j.jtice.2023.104750.

[27] S. Sardana, A. Gupta, K. Singh, A.S. Maan, A. Ohlan, Conducting polymer hydrogel based electrode materials for supercapacitor applications, J. Energy Storage. 45 (2022), 103510, https://doi.org/10.1016/j.est.2021.103510.

[28] Y. Zhang, F.Q. Bai, Y. Xie, M. Zhu, L. Zhao, D. An, D. Xue, E.B. Berda, C. Wang, G. Lu, X. Jia, D. Chao, A conjugated polymer with electron-withdrawing cyano group enables for flexible asymmetric electrochromic supercapacitors, Chem. Eng. J. 450 (2022), 138386, https://doi.org/10.1016/j.cej.2022.138386.

[29] T.H. Weng, M.G. Mohamed, S.U. Sharma, I.M.A. Mekhemer, H.H. Chou, S.W. Kuo, Rationally engineered ultrastable three-dimensional (3D) conjugated microporous polymers containing triptycene, tetraphenylethene, and benzothiadiazole units as exceptional high-performance organic electrodes for supercapacitors, ACS Appl. Energy Mater. 6 (2023) 9012–9024, https://doi.org/10.1021/acsaem.3c01933.

[30] C.Y. Chen, M.G. Mohamed, W.C. Chen, S.W. Kuo, Construction of Ultrastable porous carbons materials derived from organic/inorganic double decker silsesquioxane (DDSQ) hybrid as a high-performance electrode for supercapacitor, Mater. Today Chem. 34 (2023), 101773, https://doi.org/10.1016/j.mtchem.2023.101773.

[31] W. Yang, P. Wang, Z. Tu, L. Hou, L. Yan, B. Jiang, C. Zhang, G. Huang, F. Yang, Y. Li, Heteroatoms-doped hierarchical porous carbon with multi-scale structure derived from petroleum asphalt for high-performance supercapacitors, Carbon 187 (2022) 338–348, https://doi.org/10.1016/j.carbon.2021.11.008.

[32] W. Zhu, D. Shen, H. Xie, Effect of heteroatoms on pseudocapacitance for N/O Co-doped porous carbon in an alkaline aqueous electrolyte, Energy Fuel 37 (2023) 12467–12473, https://doi.org/10.1021/acs.energyfuels.3c02061.
[33] W. Zhang, X. Huo, X. Li, S. Park, L. Lin, S.Y. Park, G. Diao, Y. Piao, Nitrogen and sulfur Codoped porous carbon directly derived from potassium citrate and Thiourea for high-performance supercapacitors, Langmuir 38 (2022) 10331–10337, https://doi.org/10.1021/acs.langmuir.2c01863.
[34] J. Yu, X. Jia, J. Peng, B. Meng, Y. Wei, J. Hou, J. Zhao, N. Yang, K. Xie, D. Chu, L. Li, Synergistic effect of nitrogen–sulfur codoping on honeycomb-like carbon-based high-energy-density zinc-ion hybrid supercapacitors, ACS Appl. Energy Mater. 6 (2023) 2728–2738, https://doi.org/10.1021/acsaem.2c03311.
[35] Y. Lin, F. Li, X. Li, H. Zhao, G. Liu, Multifunctional template prepares N-, O-, and S-codoped mesoporous 3D hollow nanocage biochar with a multilayer wall structure for aqueous high-performance supercapacitors, ACS Appl. Energy Mater. 6 (2023) 2265–2275, https://doi.org/10.1021/acsaem.2c03427.
[36] Y. Lu, J. Liu, W. Zhao, K. Zhang, Bio-benzoxazine structural design strategy toward highly thermally stable and intrinsically flame-retardant thermosets, Chem. Eng. J. 457 (2023), 141232, https://doi.org/10.1016/j.cej.2022.141232.
[37] M.G. Mohamed, W.C. Chang, S.W. Kuo, Crown ether- and benzoxazine-linked porous organic polymers displaying enhanced metal ion and CO_2 capture through solid-state chemical transformation, Macromolecules 55 (2022) 7879–7892, https://doi.org/10.1021/acs.macromol.2c01216.
[38] M.G. Mohamed, C.C. Chen, K. Zhang, S.W. Kuo, Construction of three-dimensional porous organic polymers with enhanced CO_2 uptake performance via solid-state thermal conversion from tetrahedral benzoxazine-linked precursor, Eur. Polym. J. 200 (2023), 112551, https://doi.org/10.1016/j.eurpolymj.2023.112551.
[39] M.G. Mohamed, C.J. Li, M.A.R. Khan, C.C. Liaw, K. Zhang, S.W. Kuo, Formaldehyde-free synthesis of fully bio-based multifunctional bisbenzoxazine resins from natural renewable starting materials, Macromolecules 55 (2022) 3106–3115, https://doi.org/10.1021/acs.macromol.2c00417.
[40] M.M. Samy, M.G. Mohamed, T.H. Mansoure, T.S. Meng, M.A.R. Khan, C.C. Liaw, S. W. Kuo, Solid state chemical transformations through ring-opening polymerization of ferrocene-based conjugated microporous polymers in host–guest complexes with benzoxazine-linked cyclodextrin, J. Taiwan Inst. Chem. Eng. 132 (2022), 104110, https://doi.org/10.1016/j.jtice.2021.10.010.
[41] X. Fan, S. Li, C. Wang, Y. Deng, C. Zhang, Z. Wang, Research on fluoropyridine-based benzoxazine with high thermal stability and excellent flame retardancy for its application in coatings, Eur. Polym. J. 187 (2023), 111884, https://doi.org/10.1016/j.eurpolymj.2023.111884.
[42] J.H. Cha, S.K.S. Kumar, J.E. Noh, J.S. Choi, Y. Kim, C.G. Kim, Ultra-high-molecular-weight polyethylene/hydrogen-rich benzoxazine composite with improved interlaminar shear strength for cosmic radiation shielding and space environment applications, Compos. Struct. 300 (2022), 116157, https://doi.org/10.1016/j.compstruct.2022.116157.
[43] H. Gou, Y. Bao, J. Huang, X. Fei, X. Li, W. Wei, Development of molding compounds based on epoxy resin/aromatic amine/benzoxazine for high-temperature electronic packaging applications, Macromol. Mater. Eng. 307 (2022) 2200351, https://doi.org/10.1002/mame.202200351.
[44] Y. Zheng, K. Chen, K. Jiang, F. Zhang, G. Zhu, H. Xu, Progress of synthetic strategies and properties of heteroatoms-doped (N, P, S, O) carbon materials for supercapacitors, J. Energy Storage 56 (2022), 105995, https://doi.org/10.1016/j.est.2022.105995.
[45] J. Wang, Y. Xu, M. Yan, B. Ren, X. Dong, J. Miao, L. Zhang, X. Zhao, Z. Liu, Preparation and application of biomass-based porous carbon with S, N, Zn, and Fe heteroatoms loading for use in supercapacitors, Biomass Bioenergy 156 (2022), 106301, https://doi.org/10.1016/j.biombioe.2021.106301.
[46] B. Üstün, H. Aydın, S.N. Koç, U. Kurtan, Electrospun amorphous CoOx/C composite nanofibers doped with heteroatoms for symmetric supercapacitors, Fuel 341 (2023), 127735, https://doi.org/10.1016/j.fuel.2023.127735.
[47] A. Gopalakrishnan, S. Badhulika, Effect of self-doped heteroatoms on the performance of biomass-derived carbon for supercapacitor applications, J. Power Sources 480 (2020), 228830, https://doi.org/10.1016/j.jpowsour.2020.228830.
[48] X. Zhang, G. Yan, H. Li, Z. Li, J. Chen, L. Wang, Y. Wu, Slit needleless electrospun heteroatoms-doped hollow porous carbon nanofibers for solid-state flexible supercapacitors, J. Alloys Compd. 943 (2023), 169188, https://doi.org/10.1016/j.jallcom.2023.169188.
[49] M.G. Mohamed, S.M. Ebrahium, A.S. Hammam, S.W. Kuo, K.I. Aly, Enhanced CO_2 capture in nitrogen-enriched microporous carbons derived from Polybenzoxazines containing azobenzene and carboxylic acid units, J. Polym. Res. 27 (2020) 197, https://doi.org/10.1007/s10965-020-02179-1.
[50] P. Sharma, V. Tanwar, I. Tiwari, P.O. Ingole, L. Nebhani, Sustainable upcycling of nitrogen-enriched polybenzoxazine thermosets into nitrogen-doped carbon materials for contriving high-performance supercapacitors, Energy Fuel 37 (2023) 7445–7467, https://doi.org/10.1021/acs.energyfuels.3c00237.
[51] T. Periyasamy, S.P. Asrafali, S.C. Kim, Heteroatom-enhanced porous carbon materials based on polybenzoxazine for supercapacitor electrodes and CO_2 capture, Polymers 15 (2023) 1564, https://doi.org/10.3390/polym15061564.
[52] I. Tiwari, P. Sharma, L. Nebhani, Polybenzoxazine- an enticing precursor for engineering heteroatom-doped porous carbon materials with applications beyond energy, environment and catalysis, Mater. Today Chem. 23 (2022), 100734, https://doi.org/10.1016/j.mtchem.2021.100734.
[53] H. Zhang, L. Xu, G. Liu, Synthesis of benzoxazine-based n-doped mesoporous carbons as high-performance electrode materials, Appl. Sci. 10 (2020) 422, https://doi.org/10.3390/app10010422.
[54] J. Jiang, M. Wang, W. Zhao, H. Liu, Y. Wang, P. Song, Z. Wang, Hierarchical porous carbon materials derived from N, O, S-containing bio-based polybenzoxazine for supercapacitors, Eur. Polym. J. 191 (2023), 112054, https://doi.org/10.1016/j.eurpolymj.2023.112054.
[55] W. Shi, X. Zhao, S. Ren, W. Li, Q. Zhang, X. Jia, Heteroatoms Co-doped porous carbons from amino acid based polybenzoxazine for superior CO_2 adsorption and electrochemical performances, Eur. Polym. J. 165 (2022), 110988, https://doi.org/10.1016/j.eurpolymj.2021.110988.
[56] F. Li, Y. Li, K.S. Novoselov, F. Liang, J. Meng, S.H. Ho, H. Zhao, A. Ahmad, Y. Zhu, L. Hu, D. Ji, L. Jia, R. Liu, S. Ramakrishna, X. Zhang, Bioresource upgrade for sustainable energy, environment, and biomedicine, Nano Micro Lett. 15 (2023) 35, https://doi.org/10.1007/s40820-022-00993-4.
[57] D. Kurniawan, M.R. Rahardja, P.V. Fedotov, E.D. Obraztsova, K.K. Ostrikov, W. H. Chiang, Plasma-bioresource-derived multifunctional porous NGQD/AuNP nanocomposites for water monitoring and purification, Chem. Eng. J. 451 (2023), 139083, https://doi.org/10.1016/j.cej.2022.139083.
[58] N. Yan, B. Hu, Z. Zheng, H. Lu, J. Chen, X. Zhang, X. Jiang, Y. Wu, J. Dolfing, L. Xu, Twice-milled magnetic biochar: a recyclable material for efficient removal of methylene blue from wastewater, Bioresour. Technol. 372 (2023), 128663, https://doi.org/10.1016/j.biortech.2023.128663.
[59] W. Cai, Z. Wang, Z. Shu, W. Liu, J. Wang, J. Qiu, Development of a fully bio-based hyperbranched benzoxazine, Polym. Chem. 12 (2021) 6894–6902, https://doi.org/10.1039/D1PY01451J.
[60] R.C. Lin, S.W. Kuo, Well-defined benzoxazine/triphenylamine-based hyperbranched polymers with controlled degree of branching, RSC Adv. 8 (2018) 13592–13611, https://doi.org/10.1039/C8RA00506K.
[61] K. Zhang, M.C. Han, L. Han, H. Ishida, Resveratrol-based tri-functional benzoxazines: synthesis, characterization, polymerization, and thermal and flame retardant properties, Eur. Polym. J. 116 (2019) 526–533, https://doi.org/10.1016/j.eurpolymj.2019.04.036.
[62] Q. Zhao, X. Wang, C. Wu, J. Liu, H. Wang, J. Gao, Y. Zhang, Supercapacitive performance of hierarchical porous carbon microspheres prepared by simple one-pot method, J. Power Sources 254 (2014) 10–17, https://doi.org/10.1016/j.jpowsour.2013.12.091.
[63] Y. Liu, L. Cao, J. Luo, Y. Peng, Q. Ji, J. Dai, J. Zhu, X. Liu, Biobased nitrogen- and oxygen-Codoped carbon materials for high-performance supercapacitor, ACS Sustain. Chem. Eng. 7 (2019) 2763–2773, https://doi.org/10.1021/acssuschemeng.8b05947.
[64] L. Wan, J. Wang, L. Xie, Y. Sun, K. Li, Nitrogen-enriched hierarchically porous carbons prepared from polybenzoxazine for high-performance supercapacitors, ACS Appl. Mater. Interfaces 6 (2014) 15583–15596, https://doi.org/10.1021/am504564q.
[65] C.O. Ania, V. Khomenko, E. Raymundo-Piñero, J.B. Parra, F. Béguin, The large electrochemical capacitance of microporous doped carbon obtained by using a zeolite template, Adv. Funct. Mater. 17 (2007) 1828–1836, https://doi.org/10.1002/adfm.200600961.
[66] J. Wu, D. Zhang, Y. Wang, B. Hou, Electrocatalytic activity of nitrogen-doped graphene synthesized via a one-pot hydrothermal process towards oxygen reduction reaction, J. Power Sources 227 (2013) 185–190, https://doi.org/10.1016/j.jpowsour.2012.11.074.
[67] X. Gao, S. Yang, L. Hu, S. Cai, L. Wu, S. Kawi, Carbonaceous materials as adsorbents for CO_2 capture: synthesis and modification, Carbon Capture Sci. Technol. 3 (2022), 100039, https://doi.org/10.1016/j.ccst.2022.100039.
[68] M. Ejaz, M.G. Mohamed, W.C. Chang, S.W. Kuo, Synthesis and design of hypercrosslinked porous organic frameworks containing tetraphenylpyrazine unit for high-performance supercapacitor, J. Polym. Sci. (2023), https://doi.org/10.1002/pol.20230174.
[69] M. Ejaz, M.M. Samy, Y. Ye, S.W. Kuo, M.G. Mohamed, Design hybrid porous organic/inorganic polymers containing polyhedral oligomeric Silsesquioxane/pyrene/anthracene moieties as a high-performance electrode for supercapacitor, Int. J. Mol. Sci. 24 (2023) 2501, https://doi.org/10.3390/ijms24032501.
[70] M.G. Mohamed, S.V. Chaganti, S.U. Sharma, M.M. Samy, M. Ejaz, J.T. Lee, K. Zhang, S.W. Kuo, Constructing conjugated microporous polymers containing the pyrene-4, 5, 9, 10-tetraone unit for energy storage, ACS Appl. Energy Mater. 5 (2022) 10130–10140, https://doi.org/10.1021/acsaem.2c01842.
[71] A.O. Mousa, M.G. Mohamed, C.H. Chuang, S.W. Kuo, Carbonized aminal-linked porous organic polymers containing pyrene and triazine units for gas uptake and energy storage, Polymers 15 (2023) 1891, https://doi.org/10.3390/polym15081891.
[72] A.O. Mousa, Z.I. Lin, C.H. Chuang, C.K. Chen, S.W. Kuo, M.G. Mohamed, Rational design of bifunctional microporous organic polymers containing anthracene and triphenylamine units for energy storage and biological applications, Int. J. Mol. Sci. 24 (2023) 8966, https://doi.org/10.3390/ijms24108966.
[73] M.G. Mohamed, S.V. Chaganti, M.S. Li, M.M. Samy, S.U. Sharma, J.T. Lee, M. H. Elsayed, H.H. Chou, S.W. Kuo, Ultrastable porous organic polymers containing thianthrene and pyrene units as organic electrode materials for supercapacitors, ACS Appl. Energy Mater. 5 (2022) 6442–6452, https://doi.org/10.1021/acsaem.2c00942.
[74] M.G. Mohamed, M.M. Samy, T.H. Mansoure, S.U. Sharma, M.S. Tsai, J.H. Chen, J. T. Lee, S.W. Kuo, Dispersions of 1,3,4-oxadiazole-linked conjugated microporous polymers with carbon nanotubes as a high-performance electrode for supercapacitors, ACS Appl. Energy Mater. 5 (2022) 3677–3688, https://doi.org/10.1021/acsaem.2c00100.
[75] M.M. Samy, M.G. Mohamed, S.W. Kuo, Directly synthesized nitrogen-and-oxygen–doped microporous carbons derived from a bio-derived polybenzoxazine exhibiting high-performance supercapacitance and CO_2 uptake, Eur. Polym. J. 138 (2020), 109954, https://doi.org/10.1016/j.eurpolymj.2020.109954.